

# Intracorneal Ring Segment Implantation Results in Corneal Mechanical Strengthening Visualized With Optical Coherence Elastography

**Journal Article****Author(s):**

Torres-Netto, Emilio A.; Hafezi, Farhad; Kling, Sabine

**Publication date:**

2022-07

**Permanent link:**

<https://doi.org/10.3929/ethz-b-000559372>

**Rights / license:**

[In Copyright - Non-Commercial Use Permitted](#)

**Originally published in:**

Journal of Refractive Surgery 38(7), <https://doi.org/10.3928/1081597X-20220608-01>

**Funding acknowledgement:**

174113 - Measuring local corneal biomechanical properties by multi-frequency vibrography: Moving towards an earlier diagnosis of pathologies and personalized computer simulations (SNF)

1 **Intrastromal ring segment implantation results in corneal mechanical strengthening**  
2 **visualized with optical coherence elastography**

3

4 Emilio A. Torres-Netto<sup>1,2,3,4</sup>, MD, PhD, Farhad Hafezi<sup>1,2,4</sup>, MD, PhD, FARVO, Sabine Kling<sup>5,6</sup>,  
5 PhD

6

7 <sup>1</sup> Laboratory of Ocular Cell Biology, Center for Applied Biotechnology and Molecular Medicine,  
8 University of Zurich, Zurich, Switzerland

9 <sup>2</sup> Faculty of Medicine, University of Geneva, Geneva, Switzerland

10 <sup>3</sup> Department of Ophthalmology, Paulista School of Medicine, Federal University of Sao Paulo,  
11 Sao Paulo, Brazil

12 <sup>4</sup> ELZA Institute AG, Dietikon/Zurich, Switzerland

13 <sup>5</sup> OPTIC team, Computer Vision Laboratory, ETH Zurich, Switzerland

14 <sup>6</sup> ARTORG Center for Biomedical Engineering Research, University of Bern, Bern, Switzerland

15

16 **Word count:** 2697

17

18 **Corresponding author:**

19 Sabine Kling, OPTIC-team, Computer Vision Laboratory, Department of Information  
20 Technology and Electrical Engineering, ETH Zurich, Sternwartstrasse 7, 8092 Zurich,  
21 Switzerland, klings@ee.ethz.ch

22

23 **Financial disclosure:**

24 ET (none), FH (none), SK (none)

25

26

27

28

29

30

31 **Abstract:**

32 **Purpose:** To quantify the mechanical impact of intracorneal ring segment (ICRS) implantation  
33 of different dimensions in an *ex vivo* eye model.

34 **Methods:** A total of 30 enucleated porcine eyes were assigned to ICRS implantation  
35 (thickness 300  $\mu\text{m}$ , angle 120°, 210° or 325°), tunnel creation only or virgin control. For  
36 mechanical evaluation, each globe was mounted on a customized holder and intraocular  
37 pressure (IOP) was increased in steps of 0.5 mmHg from 15 to 17 mmHg, simulating  
38 physiologic diurnal IOP fluctuations. At each step, an optical coherence tomography volume  
39 scan was recorded. Deformations between subsequent scans, as well as the locally induced  
40 axial strains were analyzed using a vector-based phase difference method. The effective E-  
41 modulus was derived from the overall induced strain as a measure of global mechanical  
42 impact.

43 **Results:** ICRS implantation increased the effective E-modulus from 146 and 163 kPa in virgin  
44 and tunnel-only eyes to 149, 192 and 330 kPa in eyes that received a 5 mm optical zone ICRS  
45 with 120°, 210° and 325° arc length, respectively; and to 209 kPa in a 6 mm optical zone ICRS  
46 with 325° arc length. The most consistent effect was a shift towards positive strains in the  
47 posterior stroma by 0.1 to 0.46 ‰ (factor 1.15 to 2.15) after ICRS surgery.

48 **Conclusions:** ICRS implantation reduces the overall tissue strain under the load of the IOP  
49 and provokes posterior tissue relaxation. This effect is more dominant the longer the arc length  
50 and the smaller the optical zone of the ICRS is. ICRS have not only a geometrical, but also a  
51 mechanical impact on corneal tissue. This behavior might have clinical implications when  
52 ICRS implantation is performed in biomechanically weakened keratoconus corneas.

53 **Introduction:**

54 Intracorneal ring segments (ICRSs) belong to the category of additive surgery and selectively  
55 flatten the cornea to correct optical errors like myopia<sup>1</sup>, astigmatism<sup>2</sup>, and especially corneal  
56 ectatic diseases like keratoconus<sup>3</sup>. Commercially available ICRS are made of  
57 polymethylmethacrylate and manufactured in different dimensions with a thickness between  
58 150 and 350  $\mu\text{m}$ , an arc length between 90° and 360°, an optical zone between 5- and 6-mm  
59 diameter, a base width between 600 to 800  $\mu\text{m}$  and a triangular, hexagonal or oval cross-  
60 sectional shape. Ophthalmic surgeons rely on experience and on nomograms supplied by the  
61 manufacturers to select the most adequate ICRS for their patient. As a general rule, the thicker  
62 the ICRS and the smaller its optical zone, the larger is the achieved flattening effect<sup>4,5</sup>. In this  
63 context, short arc lengths better correct for astigmatism<sup>6</sup> and long arc lengths better correct  
64 for defocus. In keratoconus, the location of the cone with regard to a reference meridian and  
65 the keratoconus phenotype are additionally considered for ICRS selection.<sup>7</sup> ICRSs may be  
66 also successful in regularizing the corneal surface to facilitate contact lens fitting in severely  
67 degraded corneas<sup>8</sup>.

68 While laser ablation surgery weakens the ocular shell, the mechanical impact of ICRS  
69 implantation is still not fully understood. Daxer et al<sup>9</sup> proposed a model, in which the ICRS is  
70 considered to act as an artificial limbus leading to an overall strengthening of the cornea. On  
71 the other hand, numerical simulation studies suggest only a locally restricted mechanical  
72 impact, with negligible stress modifications in the corneal center<sup>10</sup> Although in clinical use for  
73 more than 2 decades<sup>11</sup>, to date there are no published clinical data available to demonstrate  
74 a beneficial effect of ICRS implantation for keratoconus in terms of corneal biomechanics.

75 With the advent of new imaging approaches to assess mechanical characteristics non-  
76 invasively and with high spatial resolution, we have recently demonstrated using optical  
77 coherence elastography (OCE) that in an *ex vivo* eye model corneal strain distribution in the  
78 periphery of the ICRS remains unchanged, while the posterior stroma surrounded by the ICRS  
79 experiences a shift towards positive strains, ie relaxation.<sup>12</sup> This particular OCE set-up allows

80 to observe the mechanical response of ocular tissue under a close-to-natural loading  
81 condition, which makes the interpretation of the derived strain maps directly comparable to  
82 the post-surgical refractive outcome. While stress distribution is often assessed as a measure  
83 of mechanical characterization, it is not directly accessible by imaging. However, OCE is able  
84 to assess strain (ie., displacement), which is the immediate result (deformation) of the  
85 interaction between the tissue and an applied stress field. Given that also theoretically strain  
86 is directly related to stress - in an isotropic material linearly - the strain field is a meaningful  
87 parameter to study.

88 Investigating changes in mechanical stress distribution as a consequence of ICRS  
89 implantation is also relevant with regard to the refractive outcome, given that the corneal  
90 stress-strain curve is non-linear. Local tissue relaxation thus would correspond to a local  
91 weakening, which might be crucial when evaluating the long-term stability of the refractive  
92 correction in degenerative diseases such as keratoconus. Usually, an additive surgery with  
93 ICRS is performed in moderate to advanced cases of keratoconus. Several studies show  
94 regularization of the corneal anterior surface of such cases and improvement of the corrected  
95 visual acuity. On the other hand, predictability of these treatments still must be improved a  
96 considerable, and the fact that mechanical effects are currently not taken into consideration  
97 might be one of the reasons ICRS surgery so far is less predictable<sup>11,13-15</sup> than desired.

98 The purpose of the current study was to experimentally measure the axial strain field that is  
99 induced after ICRS implantation of different dimensions and quantify the overall mechanical  
100 impact of the surgery.

101

## 102 **Methods:**

### 103 Implantation procedure

104 A total of 30 freshly enucleated porcine eyes were obtained from the local slaughterhouse  
105 (Zurich, Switzerland) and used within 8 hours. Eyes were collected from young adult pigs aged  
106 6 to 8 months and had not been steamed. All eyes showed intact epithelium and were  
107 randomly divided into 6 experimental groups (n=5 per group) (see Table 1). Whereas group 1

108 eyes served as virgin control, in eyes of groups 2 to 6, a stromal channel was created under  
109 a surgical microscope by means of a micrometer diamond knife (Duckworth & Kent Ltd.,  
110 United Kingdom) with an incision depth of 750  $\mu\text{m}$  and a manual dissector (Mediphacos, Belo  
111 Horizonte, Minas Gerais, Brazil) with a 5 mm optical zone in groups 2 to 5 and a 6 mm optical  
112 zone in group 6. Eyes of groups 3 to 6 received an ICRS (Keraring, Mediphacos) with a  
113 triangular cross-section, a thickness of 300  $\mu\text{m}$  and different arc lengths of 120°, 210° and  
114 325°, respectively, matching the optical zone of the stromal tunnel. This relatively high ICRS  
115 thickness was chosen to guarantee a pronounced effect even in the porcine cornea, which is  
116 thicker than a human cornea (878  $\mu\text{m}$ <sup>16</sup> vs 515  $\mu\text{m}$ <sup>17</sup>) for which the ICRS is designed for.

117

#### 118 Optical coherence elastography (OCE)

119 Imaging with a spectrometer based custom-built optical coherence tomography set-up with an  
120 axial and lateral resolution of 3.9 and 12.4  $\mu\text{m}$  in tissue, respectively, was performed during  
121 intraocular pressure (IOP) modulation similar as described earlier.<sup>18,19</sup> OCT measurements  
122 were performed 1 day after ICRS implantation. In the meantime, the eyes were stored in  
123 plastic bags at 4°C. To compensate IOP reduction over night and leave time to reach an  
124 equilibrium, approx. 45 min before elastographic assessment, the IOP of all eyes was adjusted  
125 to 15 mmHg. A drop of PBS (phosphate-buffered saline) was applied on the corneal surface  
126 immediately before measurement begin to prevent dehydration. For mechanical evaluation,  
127 the IOP was increased in steps of 0.5 mmHg from 15 to 17 mmHg using a needle connected  
128 to a water column and a syringe. At each pressure step, a volume scan consisting of 1000 x  
129 100 A-scans spanning over an area of 11x11 mm was recorded. Large scale motion (more  
130 than 1 pixel) between two subsequently recorded volume scans was computed using a cross-  
131 correlation approach. Subsequently, the axially induced corneal strain was determined by  
132 calculating the axial gradient of the phase difference between the two scans, following a  
133 vector-based phase approach described before.<sup>18,19</sup> In this context, axial direction refers to the  
134 direction of the OCT beam, which coincided with the optical axis of the eye. Axial compressive

135 strains are a sign of tissue compaction, and axial tensile strains indicate tissue expansion /  
136 stretching. The measurement duration of a single cornea took 5 min.

137

### 138 Data analysis

139 For a more consistent comparison between different samples, corneal thickness was  
140 normalized to 1. In order to evaluate the overall mechanical impact, the effective E-modulus  
141  $E_{eff}$  was computed. It considers the overall strain amplitude  $\Delta\varepsilon$  induced by the IOP change  
142  $\Delta_{iop}$  and the central corneal thickness  $T_{cct}$ :

$$143 E_{eff} = \frac{\Delta_{iop}}{T_{cct} \cdot \Delta\varepsilon}$$

144 For statistical analysis, data demonstrated a normal distribution. Accordingly, subsequent  
145 statistical comparisons relied on ANOVA and students t-test. A p-value of 0.05 was considered  
146 to indicate a statistical significance.

147

### 148 **Results:**

149 Corneal thickness was similar in all conditions (p=0.052 to 0.952), see Table 2. Tunnel depth  
150 in tunnel-only corneas was significantly (p=0.006 to 0.04) shallower than in corneas, in which  
151 an ICRS was implanted.

152

### 153 Optical coherence elastography

154 **Figure 1** presents the enface view of the corneal structure and axial strain distribution. As  
155 expected, the virgin and tunnel-only conditions demonstrate central tissue compression  
156 (negative axial strain, blue color) in response to IOP increase, which slightly decreased in  
157 amplitude towards the anterior stroma. In all corneas, in which an ICRS was implanted, a shift  
158 towards positive strains (ie., relaxation, warmer colors) was observed in the posterior stroma  
159 within the optical zone of the ICRS (white framed area in the posterior strain images). In the  
160 anterior cornea, the same area seemed to experience a shift towards negative strains. The  
161 size of this area did correlate well with the arc length of the ICRS.

162

163 **Figure 2 A** summarizes the mean strain across the different conditions in the central cornea,  
164 and in a 1 mm thick ring located interiorly adjoint to the ICRS. In general, the placement of an  
165 ICRS tended to reduce the strain amplitude in the posterior stroma, both in the central and  
166 ring region (blue and gray bars). This effect was stronger, the larger the arc length and the  
167 smaller the optical zone of the ICRS was. ANOVA confirmed this trend and indicated with a  
168 borderline significance of  $p=0.056$  differences in the posterior central region based on the  
169 different groups. At nearly all ICRS geometries, the increase in posterior strain was significant  
170 compared to the virgin cornea, see **Table 3**. The effective E-modulus (black continuous line,  
171 secondary y-axis) is a measure of the overall mechanical strength resulting after surgery. It  
172 showed an increase after ICRS implantation, which was largest in the ICRS with the longest  
173 arc length and smallest optical zone. Panels B and C present the strain profile as a function  
174 of stromal depth in the central and ring region, respectively. While the most anterior corneal  
175 layer demonstrated compression, the subsequent layer experienced relaxation and the  
176 remaining posterior stroma similarly got compressed. This shape of the strain profile was  
177 similar in all conditions and only the strain amplitude did vary.

178

179

## 180 **Discussion:**

181 We compare for the first-time changes in axial corneal strain after ICRS implantation of  
182 different dimensions and provide an interpretation of their global mechanical effect. We  
183 confirm that localized corneal curvature changes are mostly restricted to within the optical  
184 zone of the ICRS<sup>12</sup>.

185 The posterior stroma demonstrated a consistent decrease in strain amplitude, which can also  
186 be interpreted as a shift towards positive strains. Interestingly, such a shift towards positive  
187 strains had previously been described in corneal regions subjected to corneal cross-linking  
188 treatment.<sup>19</sup> Yet there, the shift could not be attributed to an overall decrease in strain  
189 amplitude, but rather to a shift in the strain profile. Independent of the underlying mechanism,



190 it seems that increasing the mechanical stability either by implanting a long-arc rigid ring  
191 segment, or by directly stiffening the corneal tissue causes a spatially confined tissue  
192 relaxation.

193 Recently, Daxer<sup>9</sup> has introduced a strengthening factor to quantify the mechanical effect of  
194 the ICRS by considering it acts as an artificial limbus. It needs to be considered that this factor  
195 is most accurate when evaluating the mechanical impact of a full (360° arc length) implant. In  
196 the current study, we propose the effective E-modulus as a novel measure to quantify the  
197 mechanical strengthening after ICRS implantation, also in implants of shorter arc lengths. A  
198 particular advantage of the effective E-modulus is that it does not rely on theoretical  
199 assumptions, but instead is directly related to tissue strain, and independent of corneal  
200 thickness and the applied IOP. We showed that the effective E-modulus increases by up to  
201 factor 2.25 in the 325° arc length ICRS with a 5 mm optical zone. This value comes close to  
202 the strengthening factor predicted by Daxer for a 360° ICRS suggesting that the two  
203 parameters are comparable.

204 It is important to note that both, the effective E-modulus and the strengthening factor do not  
205 suggest an actual increase in tissue stiffness. The two parameters merely use mechanical  
206 denominations to describe the joint mechanical behavior of cornea + ICRS after surgery.  
207 Given the hyper-elastic nature of the natural corneal tissue, a decrease in tissue strain results  
208 rather in (minor) tissue softening than stiffening.

209 An additional point is that significant alterations of posterior stromal strain were identified at  
210 210° and 325° arc length, but not at 120° arc length ICRS. Clinically, ICRS greater than 180°  
211 arc length usually correct more defocus. The hypothesis is that such arcs from 180 degrees  
212 on are able to exert forces on precisely contralateral areas of the cornea, thus flattening an  
213 area larger than a specific single axis, and therefore correcting more defocus and less  
214 astigmatism. Interestingly, significant increases in the estimated E-moduli were found  
215 especially in these situations of 210° and 325° arc length, where a shift towards positive strains  
216 was observed.

217 Tunnel depth was consistently shallower (33 to 60%) in the current study than typically  
218 achieved in patients (70% to 75%). This can likely be attributed to the fact that porcine corneas  
219 have been used in the current study and that the available diamond knife used for incision did  
220 not allow for deeper tunnel creation. An unexpected observation was that tunnel depth in the  
221 tunnel-only condition was persistently shallower than in eyes that received subsequent ICRS  
222 implantation ( $p < 0.05$ ). We may speculate that is an artifact related to the measurement, as  
223 tunnel depth in corneas with an ICRS was conducted once the ICRS was already in place,  
224 and also because the cutting depth on corneas was initially set to be the same. A further  
225 unexpected finding was a trend towards positive strains in the periphery of virgin corneas. This  
226 effect likely can be attributed to the inclined corneal tissue with respect to the imaging beam.  
227 In consequence, rather hoop strain than radial strain is measured, which naturally experiences  
228 tissue extension upon IOP increase.

229 Opposite to the observations of our current and our previous<sup>12</sup> study, a recent numerical study  
230 found that corneal stress after ICRS implantation<sup>10</sup> relaxed in the anterior stroma, and  
231 increased in the posterior stroma. The origin of this discrepancy likely emphasizes the  
232 complex mechanical interactions in corneal tissue and demands for more sophisticated  
233 mechanical models. On the other hand, one of the limitations of the current study is that  
234 measurements were conducted in post-mortem tissue, which reportedly is subjected to  
235 hydration artifacts arising from the degrading pumping efficacy of the endothelial cells. Thus,  
236 the discrepancy might also result from a modified hydration state. A further limitation here is  
237 that porcine corneas are approx. 1.7 times thicker<sup>16,17</sup> than healthy human corneas, and  
238 approx. 2.2 times thicker than a keratoconic human cornea. Therefore, the strain amplitude  
239 and strain pattern observed in the current study is likely not a realistic representation of a  
240 typical clinical outcome, but rather gives an impression on the underlying working principle of  
241 additive surgery. Future research is demanded to investigate the effect of ICRS implantation  
242 directly *in vivo* in patients.

243

244 In conclusion, the current study quantifies the overall mechanical strengthening effect resulting  
245 after ICRS implantation of different dimensions and confirms a distinct effect in the anterior  
246 and posterior stroma. ICRS implantation reduces the overall tissue strain under the load of  
247 the IOP and provokes posterior tissue relaxation, that is more dominant in longer arc lengths  
248 and smaller optical zone ICRSs. ICRS have not only a geometrical, but also a mechanical  
249 impact on corneal tissue, which might impact the clinical behavior in eyes implanted with ICRS.

250

251

252 **Acknowledgement:**

253 This study received funding from the Swiss National Science Foundation (Ambizione  
254 PZ00P2\_174113 to SK). The authors thank Mediphacos (Belo Horizonte, MG, Brasil) for  
255 sponsoring the intrastromal ring segments and the surgical kit required for implantation.

256

257

258 **Author contributions:**

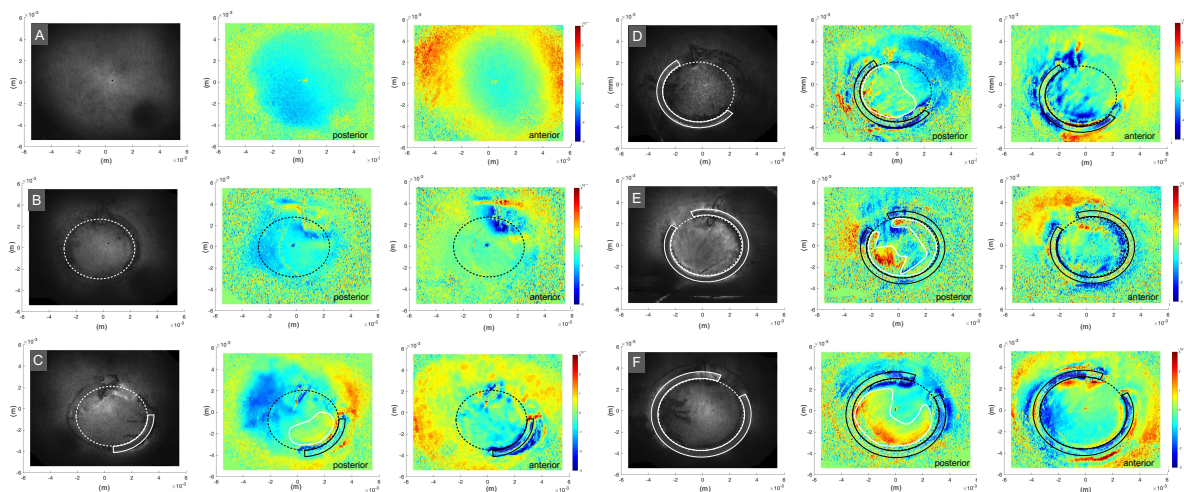
259 **EATN:** designed the study, performed the ICRS surgery, data interpretation, revised the  
260 manuscript.

261 **FH:** provided surgical equipment and advise, revised the manuscript.

262 **SK:** conceived and designed the study, conducted the elastography measurements, data  
263 processing and interpretation, drafted the manuscript, obtained funding.

264

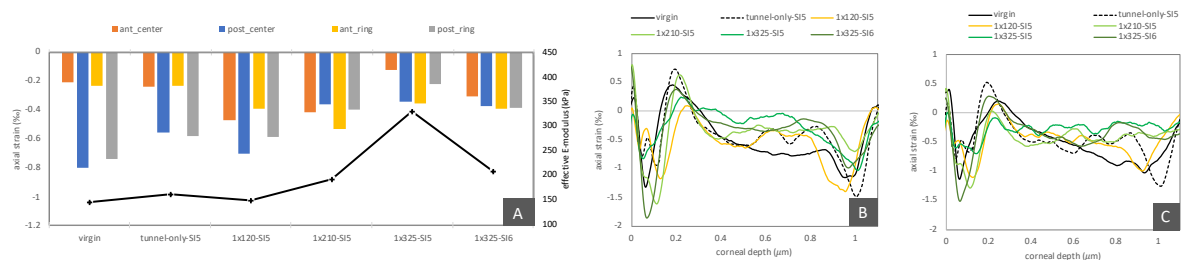
265 **Figure, Tables and Captions**



266

267 **Figure 1.** Representative images of the different conditions (A) virgin – group 1, (B) tunnel-  
 268 only – group 2, (C) 120° arc length ICRS with an optical zone of 5 mm – group 3, (D) 210° arc  
 269 length ICRS with an optical zone of 5 mm – group 4, (E) 325° arc length ICRS with an optical  
 270 zone of 5 mm – group 5, (D) 325° arc length ICRS with an optical zone of 6 mm – group 6. At  
 271 each letter, the first panel presents the structural image together with the indicated location of  
 272 the stromal tunnel (dashed white line) and the ICRS (continuous white line). The second and  
 273 third panel present the mean axial strain distribution in the posterior and anterior stroma,  
 274 respectively. The white framed area in the posterior strain images indicates the region in which  
 275 a shift towards positive strains (i.e. relaxation) was observed.

276



277

278 **Figure 2.** (A) Mean axial strain in the central and ring region interior to the ICRS in the different  
 279 conditions. The black line represents the effective E-modulus. Axial strain profile as a function  
 280 of stromal depth in (B) the central and (C) the ring region - interiorly adjoint to the ICRS.

281 ant\_center = anterior central region; post\_center = posterior central region; ant\_ring = anterior  
 282 ring region; post\_ring = posterior ring region;

283

284

285 **Table 1.** Summary of the different conditions analyzed in this study.

group	condition	optical zone (mm)	ICRS thickness ( $\mu$ m)
1	virgin	-	-
2	tunnel-only	5	-
3	1x120	5	300
4	1x210	5	300
5	1x325	5	300
6	1x325	6	300

286

287

288 **Table 2.** Summary of corneal and tunnel thickness in the analyzed groups

condition	thickness	tunnel depth	ratio
virgin	1180	-	-
tunnel-only	1174	391	0.33
1x120-SI5	1178	645	0.55
1x210-SI5	1257	636	0.51
1x325-SI5	1257	624	0.49
1x325-SI6	1191	708	0.60

289

290

291 **Table 3.** Statistical comparison of posterior stromal strain between different conditions. Bold  
 292 print indicates a statistical significant difference with  $p < 0.05$ .

293

	virgin	tunnel- only-SI5	1x120-SI5	1x210-SI5	1x325-SI5	1x325-SI6
virgin	-					
tunnel-only-SI5	0.140	-				
1x120-SI5	0.662	0.532	-			
1x210-SI5	<b>0.044</b>	0.267	0.162	-		
1x325-SI5	<b>0.017</b>	0.082	0.115	0.917	-	

1x325-SI6	0.024	0.216	0.124	0.933	0.822	-
-----------	-------	-------	-------	-------	-------	---

294

295

296 **References:**

297 1. Schanzlin, D. J., Asbell, P. A., Burriss, T. E. & Durrie, D. S. The Intrastromal Corneal Ring  
 298 Segments: Phase II Results far the Correction of Myopia. *Ophthalmology* **104**, 1067–  
 299 1078 (1997).

300 2. Arriola-Villalobos, P. *et al.* Intrastromal corneal ring segment implantation for high  
 301 astigmatism after penetrating keratoplasty. *J. Cataract Refract. Surg.* **35**, 1878–1884  
 302 (2009).

303 3. Miranda, D. *et al.* *Ferrara intrastromal corneal ring segments for severe keratoconus.*  
 304 (Slack Incorporated Thorofare, NJ, 2003).

305 4. Kling, S. & Marcos, S. Finite-element modeling of intrastromal ring segment implantation  
 306 into a hyperelastic cornea. *Invest. Ophthalmol. Vis. Sci.* **54**, 881–889 (2013).

307 5. Giacomini, N. T. *et al.* Intracorneal ring segments implantation for corneal ectasia. *J.*  
 308 *Refract. Surg.* **32**, 829–839 (2016).

309 6. Ruckhofer, J., Stoiber, J., Twa, M. D. & ünther Grabner, G. Correction of astigmatism  
 310 with short arc-length intrastromal corneal ring segments: preliminary results.  
 311 *Ophthalmology* **110**, 516–524 (2003).

312 7. Fernández-Vega Cueto, L. *et al.* Intrastromal corneal ring segment implantation in 409  
 313 paracentral keratoconic eyes. *Cornea* **35**, 1421–1426 (2016).

314 8. Moreira, L. B., Bardal, R. A. C. & Crisigiovanni, L. R. Contact lenses fitting after  
 315 intracorneal ring segments implantation in keratoconus. *Arq. Bras. Oftalmol.* **76**, 215–  
 316 217 (2013).

317 9. Daxer, A. Biomechanics of corneal ring implants. *Cornea* **34**, 1493 (2015).

318 10. Ariza-Gracia, M. Á., Flecha-Lescún, J., Büchler, P. & Calvo, B. Corneal biomechanics  
 319 after intrastromal ring surgery: Optomechanical in silico assessment. *Transl. Vis. Sci.*  
 320 *Technol.* **9**, 26–26 (2020).

- 321 11. Colin, J., Cochener, B., Savary, G. & Malet, F. Correcting keratoconus with intracorneal  
322 rings. *J. Cataract Refract. Surg.* **26**, 1117–1122 (2000).
- 323 12. Torres-Netto, E. A. & Kling, S. Corneal strain induced by intrastromal ring segment  
324 implantation visualized with optical coherence elastography. *Press J. Refract. Surg.*
- 325 13. Tunc, Z., Deveci, N., Sener, B. & Bahcecioglu, H. Anneaux intracorneés (Intacs) pour  
326 le traitement de l'astigmatisme asymétrique du k ratoc ne: recul de plus de deux ans. *J.*  
327 *Fr. Ophtalmol.* **26**, 824–830 (2003).
- 328 14. Wachler, B. S. B. *et al.* Intacs for keratoconus. *Ophthalmology* **110**, 1031–1040 (2003).
- 329 15. Pe a-Garc a, P., Vega-Estrada, A., Barraquer, R. I., Burguera-Gim nez, N. & Alio, J. L.  
330 Intracorneal ring segment in keratoconus: a model to predict visual changes induced by  
331 the surgery. *Invest. Ophthalmol. Vis. Sci.* **53**, 8447–8457 (2012).
- 332 16. Sanchez, I., Martin, R., Ussa, F. & Fernandez-Bueno, I. The parameters of the porcine  
333 eyeball. *Graefes Arch. Clin. Exp. Ophthalmol.* **249**, 475–482 (2011).
- 334 17. OLSEN, T. & EHLERS, N. The thickness of the human cornea as determined by a  
335 specular method. *Acta Ophthalmol. (Copenh.)* **62**, 859–871 (1984).
- 336 18. Kling, S., Khodadadi, H. & Goksel, O. Optical Coherence Elastography-Based Corneal  
337 Strain Imaging During Low-Amplitude Intraocular Pressure Modulation. *Front. Bioeng.*  
338 *Biotechnol.* **7**, (2019).
- 339 19. Kling, S. Optical coherence elastography by ambient pressure modulation for high-  
340 resolution strain mapping applied to patterned cross-linking. *J. R. Soc. Interface* **17**,  
341 20190786 (2020).

342

343